Optically Loaded Strontium Lattice Clock With a Single Multi-Wavelength Reference Cavity

Matteo Barbiero, Davide Calonico, Filippo Levi, and Marco G. Tarallo

***Abstract*— We report on the realization of a new compact strontium optical clock using a 2-D magneto-optical-trap (2D-MOT) as cold atomic source and a multi-wavelength cavity as the frequency stabilization system. All needed optical frequencies are stabilized to a zero-thermal expansion high-finesse optical resonator and can be operated without frequency adjustments for weeks. We present the complete characterization of the apparatus. Optical control of the atomic source allows us to perform low-noise clock operation without atomic signal normalization. Long- and short-term stability tests of the clock have been performed for the ^{88}Sr bosonic isotope by means of interleaved clock operation. Finally, we present the first preliminary accuracy budget of the system.**

***Index Terms*— Atomic spectroscopy, laser stabilization, optical frequency metrology, optical frequency standard, optical lattice clock, strontium.**

I. Introduction

OPTICAL lattice clocks (OLCs) based on neutral atoms are at the forefront of frequency metrology, exceeding current SI primary frequency standards of more than two orders of magnitude both in stability [1], [2] and accuracy [3]. Therefore, OLCs are suitable candidates for future redefinition of the unit of time [4]. Among several candidates, strontium is one of the most widespread atomic species in metrological and ultracold research laboratories. Because of its simple electronic structure and its commercial accessible cooling transitions, it finds successful application for optical clocks [5], [6], quantum control and quantum simulation [7], [8], probing new physics beyond the standard model [9], and chronometric geodesy [10]–[12].

OLCs are essentially composed of three main parts: 1) the optical local oscillator, with its local frequency reference usually consisting of an ultrastable passive optical resonator; 2) the atomic frequency discriminator, which is a complex ultracold atomic apparatus to cool and trap atoms in tens of μK-deep optical lattices; and 3) a self-referenced optical frequency comb for frequency measurement and comparison.

Concerning the preparation of the atomic frequency discriminator, efficient laser cooling and trapping of ultracold atoms requires additional subsystems for laser frequency stabilization and, in the case of the narrow $^1S_0$–$^3P_1$ Sr intercombination transition, spectral narrowing. This makes the OLC a rather complex system. Previous approaches to build compact and transportable OLCs tackled this problem by simplifying the frequency stabilization scheme using a monolithic multicavity [13], subharmonic frequency dissemination of remote frequency references on a telecom network and subsequent optical phase-locked loops [14], or a single multicolor ultrastable cavity [15]. Furthermore, fast loading rates of the atomic sample are realized using Zeeman slowers or direct line-of-sight collimated atomic sources, whose collisions with trapped atoms limit both the trapping lifetime and the systematic uncertainty [16] if an in-vacuum shutter is not used.

In this work, we present a Sr optical atomic clock apparatus which simplifies the atomic frequency discriminator system. We use an optically controlled cold atomic beam source based on a sideband-enhanced 2-D magneto-optical trap (2D-MOT) [17] and a multi-wavelength frequency stabilization system, which also provides the short-term stability to the clock laser source. We study the stability and reliability of the apparatus using the bosonic ^{88}Sr isotope, which possess the highest natural abundance, by means of the magnetic-field-induced spectroscopy (MIS) method [18].

This article is organized as follows. We first describe the multi-wavelength frequency stabilization system (see Section II), its stability performances, and its use for clock laser stabilization. Then we present the atomic cooling and trapping apparatus (see Section III) where we perform efficient two-stage magneto-optical trapping (MOT) and loading into a "magic wavelength" optical lattice [19]. Finally, we show the results of Sr OLC operating on the forbidden $^1S_0$–$^3P_0$ transition by the MIS method (see Section IV).

II. Compact Multi-Wavelength Frequency Stabilization System

Our multi-wavelength frequency stabilization system is schematically shown in Fig. 1. The core of the system consists of a monolithic, cylindrical optical cavity of length $L = 10$ cm and diameter $\phi = 5$ cm, made by ULE [20]. The high-reflectivity coating of the ULE mirrors features three peaks at 922, 813, and 689 nm. These correspond to the three main cooling and trapping wavelengths. The highest design finesse, about $1.6(4) \times 10^4$, is reached for the narrow $^1S_0$–$^3P_1$ intercombination transition wavelength at 689 nm, while the

Manuscript received November 25, 2021; revised March 4, 2022; accepted March 22, 2022. Date of publication April 6, 2022; date of current version April 22, 2022. This work was supported in part by the European Union' Horizon 2020 Research and Innovation Program and the EMPIR Participating States through the project EMPIR-USOQS and in part by the QuantERA Project Q-Clocks. The Associate Editor coordinating the review process was Yang Bai. *(Corresponding author: Marco G. Tarallo.)*

The authors are with the Quantum Metrology and Nanotechnologies Division, INRIM-Istituto Nazionale di Ricerca Metrologica, 10135 Torino, Italy (e-mail: m.tarallo@inrim.it).

Digital Object Identifier 10.1109/TIM.2022.3165292

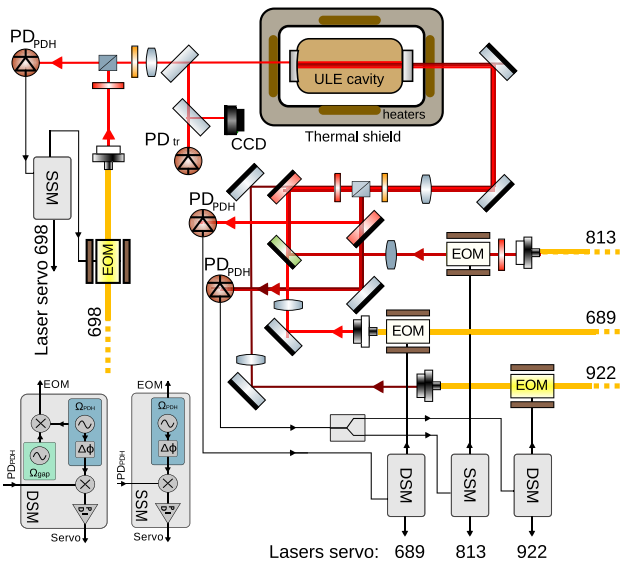

Fig. 1. Schematic drawing of the multi-wavelength frequency stabilization system for a strontium OLC. Red (green) mirrors represent long-(short-) pass optical filters. PD: photodetector. SSM: single-sideband modulation/demodulation electronic circuit. DSM: dual sideband. Details in the main text.

other two wavelengths (first cooling stage and lattice trapping) have finesse of $3.2(4) \times 10^3$.

The cavity sits on a V-shaped support over four viton balls inside a stainless-steel vacuum tank. This, in turn, is thermally decoupled from the optical table by two Teflon supports. High vacuum (about 1×10^{-8} mbar) is maintained by a 20-L/s ion pump. The temperature of the cavity is actively stabilized to its zero coefficient of thermal expansion (CTE) point at 29.34 °C by means of one polyimide thermofoil heater and two silicon rubber heaters attached to the three sides of the cylindrical-shaped vacuum system. Several layers of polyurethane foam ensure thermal insulation. A digital proportional–integral–derivative servo loop keeps the vacuum tank temperature at the desired value within 5 mK.

Photothermal effects and residual temperature fluctuations can further limit the frequency stability of a laser locked to the optical cavity. These effects have been considered and described in Sections II-C and IV-B.

A. Cooling and Trapping Lasers' Frequency Stabilization

The two lasers needed for laser cooling of ^{88}Sr at 461 and 689 nm are frequency-referenced to the multi-wavelength cavity by means of the dual-sideband offset locking technique [21]. This modified version of the Pound–Drever–Hall (PDH) technique allows us to tune the carrier frequency independently of the cavity resonance by shifting the modulation frequency Ω_{gap}. The PDH signal is extracted by demodulating the photodiode signal at the second sideband Ω_{PDH}. Together with the lattice laser at 813 nm, all these three laser beams are sent to the same side of the cavity and share the same optical path and polarization optics, as shown in Fig. 1. The 689-nm reflected beam is separated from the other two beams by another short-pass mirror and then detected with a PDH photodetector. For the other two wavelengths, the error signal is generated from the photocurrent of the same photodiode by frequency demodulation at their respective Ω_{PDH} frequencies.

The 689-nm laser for the narrow $^1S_0$–$^3P_1$ intercombination transition is a commercial extended cavity diode laser (ECDL, Toptica DLPRO). It is partially sent to the multi-wavelength cavity through a polarization-maintaining (PM) optical fiber and phase-modulated by a fiber-coupled, wideband, electrooptic modulator (EOM, Jenoptik PM705).

The dual-sideband modulation is generated by electronic mixing of two RF oscillators at $\Omega_{\text{gap}} \sim 166$ MHz and $\Omega_{\text{PDH}} = 10.5$ MHz, respectively, so that the carrier has no phase modulation at Ω_{PDH}. Each offset sideband takes typically 24% of the total power sent to the cavity, which is about 45 μW. This corresponds to a modulation index nearly equal to 1. The correction frequency is then fed back to both the ECDL's piezotransducer for low-frequency corrections and the diode current modulation input through a passive electrical network. Typical servo bandwidths of 600 kHz are achieved, so that laser low-frequency instability is dominated by the instability of the cavity.

The 461-nm light necessary for the $^1S_0$–$^1P_1$ transition is generated by a frequency-duplicated commercial diode laser (LEOS Solutions). We take a pick-off of the 922-nm subharmonic decoupled from the main beam by an optical isolator and we send it to the multi-wavelength cavity from a PM fiber and a fiber EOM. The offset sideband frequency is tuned to 189.9 MHz while the second sideband is at 13.33 MHz. About 30 μW of optical power is sent to the cavity with a carrier-to-offset sideband power ratio of 27%. In this case, the correction signal is fed back only to the ECDL's piezotransducer for slow correction of the seed wavelength.

The lattice laser (Ti:Sapph) at 813 nm is frequency-stabilized to the multi-wavelength cavity with standard PDH technique on the nearest cavity resonance to the known magic frequency [22], with a stability exceeding 100 kHz.

B. Clock Laser Frequency Stabilization

The clock laser at 698 nm is also a commercial ECDL (Toptica DLPRO) delivering up to 35 mW of optical power. It is currently frequency-stabilized to the multi-wavelength cavity, entering from the opposite side of the cavity with respect to 689 nm and other cooling lasers, as shown in Fig. 1. To avoid unwanted cross-talks with the close 689-nm laser light transmitted from the cavity, the input circular polarization is carefully tuned with opposite sign. We send 20 μW of optical power phase-modulated at $\Omega_{\text{PDH}} = 23$ MHz, far from any harmonics of the other RF frequencies.

The clock laser is locked to cavity with the standard PDH technique. The servo loop is similar to the one described for the 689-nm laser, with correction sent to both the diode current and the ECDL piezotransducer. In this case, the control bandwidth exceeds 1.2 MHz, with the in-loop error signal reaching the detector noise floor (85 mHz/$\sqrt{\text{Hz}}$) up to 20 kHz.

C. Stability Results

The frequency stability of an optical resonator of ULE, which is temperature-stabilized to its zero CTE point,

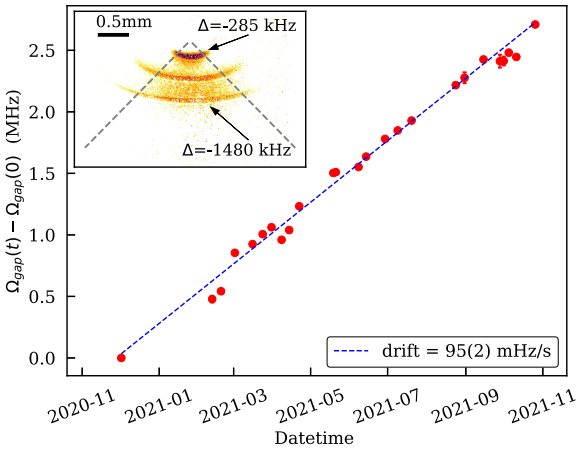

Fig. 2. Long-term frequency stability of the multi-wavelength cavity measured for an 11-month period by monitoring the offset sideband Ω_{gap} used in the frequency stabilization loop of the $^1S_0$–$^3P_1$ transition laser. In the inset, absorption images of the red MOT show transverse dimension dependence at different detunings Δ.

is limited by the aging of the spacer material, resulting is a slow drift [23]. We developed a method to track this long-term drift with respect to the resonance transition $^1S_0$–$^3P_1$ necessary for the second-stage ultracold MOT of the atomic sample (see Section III). We infer the $^1S_0$–$^3P_1$ resonant frequency by imaging the red MOT with respect to the offset sideband frequency Ω_{gap} and then fitting the transverse dimension of the atomic cloud, which linearly depends on cooling frequency detuning [24] as shown in the inset of Fig. 2. The main panel of Fig. 2 reports the recorded values of Ω_{gap} at which the 689-nm laser is on resonance with respect to the $^1S_0$–$^3P_1$ transition over a period of 11 months. We infer an average drift rate of 95(2) mHz/s (or 2×10^{-11} /day in relative units). This low drift value allows us to prepare and manipulate ultracold samples of Sr atoms without any frequency adjustment for weeks.

The stability of the multi-wavelength cavity as frequency reference is limited by vibration-induced length fluctuations δL_v induced by axial and transverse cavity accelerations a_{axial} and a_{trans}. This can be parameterized as [25]

$$\frac{\delta L_v}{L} = \frac{\rho}{2Y}(\epsilon L a_{\text{axial}} + a_{\text{trans}}\phi\sigma) \tag{1}$$

where ρ is the cavity spacer density, σ and Y are the Poisson' ratio and Young's modulus, respectively, and ϵ parameterizes the acceleration transmissivity due to the cavity support geometry, ranging from 0 to 1 [26]. No antivibration measures are taken for our cavity, so that for typical ambient seismic noise we can estimate the induced frequency instability. Assuming a typical environmental acceleration noise spectral density $\delta a(f) \sim 5 \times 10^{-5}$ ms$^{-2}/\sqrt{\text{Hz}}$ [27], [28] up to few hundred hertz, and a sensitivity coefficient $\epsilon = 0.5$, the expected vibration-limited fast linewidth is expected to be about 10 Hz.

An important detrimental effect that could limit the frequency stability of a laser, and in particular the clock laser, to the multi-wavelength cavity is the length fluctuations due to other lights' intensity noise. While we do not expect that this effect limits our clock laser, due to the noncompensated vibration noise, it is interesting to evaluate this effect for future implementations of the system with higher frequency stability requirements. To estimate the transmitted intensity noise from other lasers to the clock light, we modulated the amplitude of the RF power generating the offset sidebands Ω_{gap} for the 689- and 922-nm lights and we looked at the corresponding frequency shift with respect to a high-stability optical oscillator [29]. From a linear fit of the cavity frequency shifts against the transmitted power, we infer cavity shift coefficients of $k_{689} = 4(1)$ Hz/μW and $k_{922} = 2(2)$ Hz/μW, respectively. The shift measurement for the 922-nm light is compatible with zero. These results can be explained as due to the heating of the dielectric mirror coating generated by the intracavity optical power at different wavelengths [28], [30]. For our system, this results in frequency instability $\sigma_y(\tau) = 1.1(4) \times 10^{-16}\sqrt{\tau}$ for an intracavity relative intensity noise of 0.3%.

The short-term stability of the multi-wavelength frequency stabilization system is best studied for clock laser by looking at its effect on clock spectroscopy and clock stability via the Dick effect [31]. This is described in detail in Section IV-B.

III. Cooling, Trapping, and Probing Apparatus

A schematic overview of our atomic cooling and trapping apparatus is shown in Fig. 3. It consists of two main parts, the 2D-MOT atomic source and the science cell setup.

The cold atomic source of this apparatus, as well as the details on the complete vacuum system, has been extensively described in [17]. Here, we briefly recall the main properties of the system. A cold, bright atomic beam is generated by a two-frequency 2D-MOT transversely loaded from a collimated Sr oven (typically operated at 460 °C), with an average longitudinal velocity of 22 m/s and a transverse temperature of less than 1 mK. This allows us to achieve a loading rate in the science chamber up to 8×10^8 atoms/s, tunable by changing the optical power of the push beam.

Such cold atomic beam is then cooled and trapped in the science cell, where 3-D magneto-optical cooling and trapping is performed before loading the atomic ensemble into the optical lattice for clock spectroscopy. The overall procedure for probing the $^1S_0$–$^3P_0$ transition by means of MIS technique is depicted in Fig. 3(c).

A. Laser Cooling of ^{88}Sr Atoms

In the science chamber, the atoms from the atomic source are loaded in the "blue MOT" operated on the $^1S_0$–$^1P_1$ at 461 nm for 100 ms. We typically apply a total intensity $s = 0.88$ (in units of the resonant saturation intensity) and a magnetic field gradient of 4 mT/cm. Switching off the push beam interrupts the atomic flux. The MOT is operated for additional 20 ms. This covers both the time-of-flight of the remaining atoms from the 2D-MOT and a short MOT phase (5 ms) at reduced intensity ($s = 0.26$) to further cool down the collected sample. At the end, we collect up to 7×10^6 atoms at 2(1) mK. All the laser beams at 461 nm and the magnetic

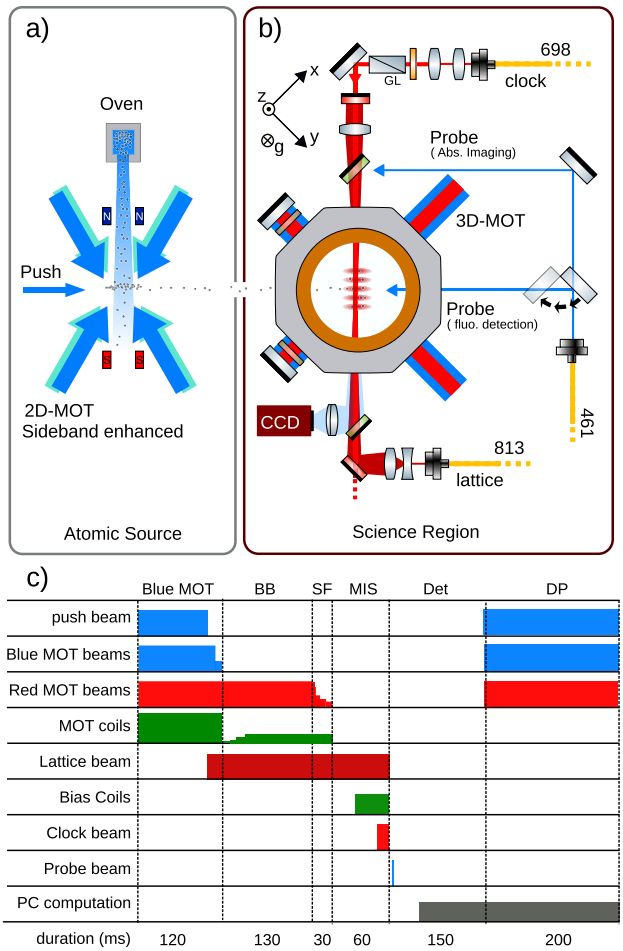

Fig. 3. Schematic drawing of the OLC system and its experimental procedure. (a) Atomic source region, (b) science cell and schematic layout for atomic interrogation, and (c) clock interrogation procedure. BB: Broadband red MOT phase. SF: Single-frequency red MOT phase. MIS: Magnetic-induced spectroscopy. Det.: Detection. DP: Data processing.

field gradient are then switched off, and we use a mechanical shutter to completely turn off the blue light.

The second cooling stage is performed on the $^1S_0$–$^3P_1$ intercombination transition ("red" MOT [24]) at 689 nm. We initially use about 13 mW of optical power ($s \sim 2 \times 10^3$) with a broadband (BB) spectrum to cover the majority of the Doppler spectrum of the atoms released from blue MOT. A double-pass acousto-optic modulator (AOM) yields the broadened spectrum with an FM frequency of 35 kHz, modulation depth of 3 MHz, and a minimum detuning of −400 kHz from atomic resonance. During the BB red MOT phase, the magnetic field gradient is ramped up to 1.3 mT/cm in 26 ms. The atomic density and cloud dimensions reach their stationary values in 130 ms. At the end of the BB phase, we trap up to 4×10^6 atoms at 11 μK.

Finally, the temperature of the atomic sample is further reduced by a single-frequency (SF) red MOT phase. Here, the optical power is exponentially ramped down from 13 mW to 10 μW ($s = 10$) in 30 ms. At the end of this cooling stage, we trap 3.5×10^6 atoms below 1 μK. Also for the 689-nm light, a mechanical shutter is used to avoid residual stray light going to the atoms in the optical lattice.

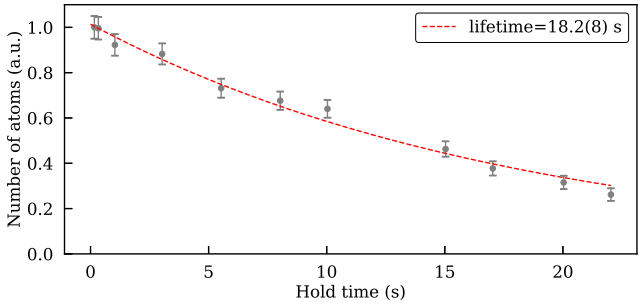

Fig. 4. Numbers of atoms in the optical lattice as a function of different hold time. The number of atoms is normalized to their maximum value.

During the whole red MOT, the optical lattice beam is turned on, so that the atoms overlapped to the lattice beam remain trapped and ready for clock spectroscopy at the switching off of the red beams and the magnetic field gradient. The total duration of the cooling and trapping is about 300 ms.

B. Magic Wavelength Optical Lattice

The optical lattice trap is realized with 500 mW of optical power at the magic wavelength of 813 nm, delivered with a PM optical fiber. The beam is shaped to produce a beam waist of about 50 μm in correspondence of the red MOT center. The lattice axis is orthogonal to the gravity direction as shown in Fig. 3. The lattice retro-reflection dichroic mirror is carefully aligned maximizing the amount of power coupled back to the fiber collimator. Up to 4×10^5 atoms can be loaded in the lattice trap with a measured lifetime of 18.2(8) s, as plotted in Fig. 4. This value is dominated by the off-resonant scattering ($\Gamma_{sc}^{-1} \approx 33$ s [32]), and therefore vacuum-limited lifetime can be as high as 40 s. This exceptionally long lattice lifetime is a consequence of the 2D MOT loading that allows us to completely turn off the atomic flux during lattice spectroscopy and also maintaining much higher differential vacuum between the two chambers in comparison to a classic Zeeman slower [33].

Time-of-flight absorption imaging measurements of the atomic sample show temperatures lower that 2 μK in both the transverse directions, while the axial free expansion of the atomic cloud is parallel to the imaging beam, and thus the axial temperature is not measurable with this method. The transverse size of the optical lattice can be extracted from temperature measurements [32], and it is about $\sigma_r = 14$ μm. The axial dimension is not accessible by the imaging system, and it is roughly estimated equal to twice the red MOT radius, about 400 μm.

The optically controlled atomic source combined with the cooling and trapping process yields a lattice population fluctuation as low as 3% for maximum loading rate, which nearly doubles at low loading rates. This number fluctuation is nearly half of the one observed when the 461-nm laser was frequency-stabilized to an atomic vapor [17].

C. Magnetic-Field-Induced Spectroscopy Setup

MIS is enabled by an homogeneous bias magnetic field applied by inverting the current of one of the MOT coils, thus

switching from antiHelmholtz to Helmholtz configuration. The bias magnetic field is directed along the gravity direction and orthogonal to the lattice beam propagation direction.

The clock laser beam at 698 nm is directed toward the atoms from the dichroic retro-reflection lattice mirror (high reflective at 813 nm and high transmissive, ~90%, at the clock wavelength). The clock laser beam is shaped to have a waist of 150 μm, i.e., three times the lattice beam waist, to ensure high homogeneity on the atoms. Clock light standing waves are avoided using a second dichroic mirror along the optical path of the input lattice beam, as depicted in Fig. 3(b). We carefully align the clock beam to the atoms by maximizing the amount of power injected to the fiber collimator of the lattice beam. Linear polarization parallel to the magnetic field is ensured by a Glan–Thomson polarizer placed before the lattice retro-reflection mirror. Finally, power and duration of the clock laser pulse are controlled by an AOM before the input fiber.

A second AOM driven by an externally referenced RF oscillator (working around 345 MHz) is used to tune the frequency of the clock laser for clock spectroscopy scans and frequency stabilization by FM modulation. The RF oscillator is directly controlled by an analog output generated by the experiment control system [34].

D. Atomic Detection Setup

Atomic detection and diagnostics is performed by the imaging system. It consists of a charge-coupled device (CCD) camera (Stingray F-201, 1624 × 1234 pixels and 4.4-μm pixel size) and an achromatic lens $f = 100$ mm displaced to get a numerical aperture of 0.10(4) and magnification factor of 0.617(3). A probe beam, resonant with the $^1S_0$–$^1P_1$ strong transition, can be either sent to the CCD camera for absorption imaging of the atomic sample or directed orthogonally to the absorption axis for fluorescence detection by means of a removable mirror. The absorption imaging optical path is integrated along the lattice direction by means of two dichroic mirrors. Residual light from the lattice and clock laser beams are then blocked by an interference filter peaked at 461 nm, mounted in front of the CCD camera.

While absorption imaging is best suited for the atomic sample diagnostics (atomic cloud dimension, temperature, and calibrated atomic count), we perform fast fluorescence imaging for clock spectroscopy. In this case, the probe beam pulse has a duration of 0.7 ms and optical power of 3 mW, while its linear polarization maximizes the atomic fluorescence toward the CCD. The CCD camera exposure time is 220 μs, while the image is downloaded to the computer control in less than 50 ms. Only 3% of the total CCD array is used to speed-up the data download and processing. Within the same image, we define two regions of interest (ROIs) with equal areas. One of the ROIs covers the majority of the atomic cloud and provides the photon counts, and the other is placed at the corner of the image and provides the background signal of the CCD. The difference between the ROIs' counts provides the fluorescence counts. The detected fluorescence signal is maximized by releasing the atoms from the lattice and probing the atoms after 4 ms of free fall.

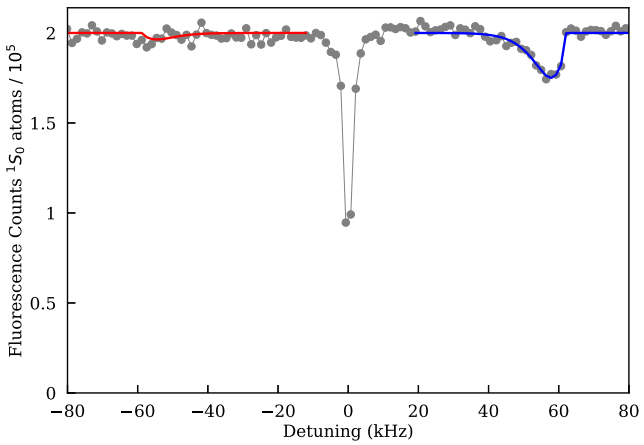

Fig. 5. Sideband-resolved spectroscopy of the ^{88}Sr clock transition. The trace is the average over four consecutive frequency scans. Motional sidebands (blue and red curves) are simultaneously fitted [35] to estimate the trap depth and the apparent radial and axial temperatures.

Almost 200 ms are spent by the computer control to manage CCD data processing and to generate the feedback signal to keep the system on the resonance of the $^1S_0$–$^3P_0$ transition. This represents the current limit for the duration of the experimental cycle. To further shorten the clock cycle, we are planning to implement a parallel processing of the CCD data within the preparation time of the atoms in the optical lattice trap.

IV. Results

A. Resolved Sideband Spectroscopy

We perform high-resolution MIS of the ^{88}Sr clock transition $^1S_0$–$^3P_0$ in the Lamb–Dicke regime with motion resolved from the carrier. An example of the sideband spectrum is presented in Fig. 5. Here, the bias coils are driven at a maximum current $I_{\text{coil}} = 10$ A, and a pulse duration of 60 ms is used to maximize the excitation of the motional sidebands. With a typical lattice optical power of 450 mW, we measure an axial trapping frequency of 65.5(2) kHz, implying a lattice depth $U_0 = 92.7(5)E_r = 15$ μK, where $E_r = h^2/(2m\lambda_L^2)$ is the lattice recoil energy. The Lamb–Dicke parameter η associated with our lattice trap depth is $\eta = 0.26$.

We also measure the apparent axial (T_z) and radial (T_r) temperatures of the atomic sample from the shape and relative areas of the first-order motional sidebands [35]. The resulting temperatures are $T_r = 3.2(3)$ μK and $T_z = 1.6(3)$ μK. Compared with time-of-flight temperature measurement, the apparent radial temperature is slightly higher (~2 μK), implying either the simplicity of the fitting function which does not include any broadening effect or an underlying heating mechanism due to photon-assisted collisions.

B. Narrow-Line Spectroscopy and Clock Stability Test

High-resolution Rabi spectroscopy is realized by exciting the clock transition at the actual π pulse for each configuration of magnetic field and probe intensity. The resulting linewidth can be narrowed by decreasing either (or both) the bias magnetic field or the probe power. Furthermore, because of

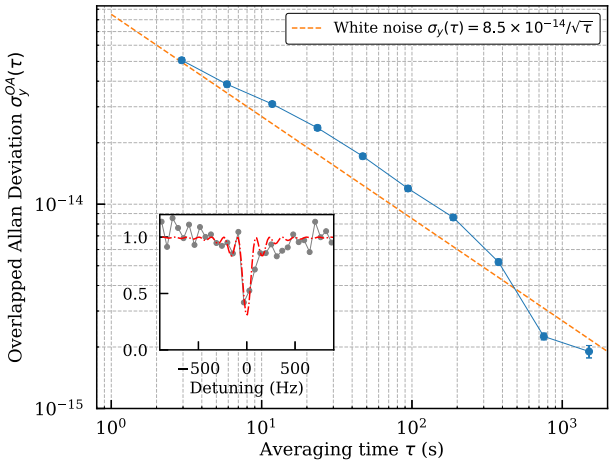

Fig. 6. Main panel: Allan deviation of the difference between two interleaved stabilizations at $N_{at} = 1.5 \times 10^5$ and 3×10^5. The dataset covers a time span of 62 min. Inset panel: Narrow-line spectroscopy of the $^1S_0$–$^3P_0$ clock transition fitted with a Rabi response function. The corresponding FWHM $\approx 1.067\ \Omega = 86(7)$ Hz.

collisional dephasing, narrow lines have to be obtained by lowering the lattice site density reducing the number of loaded atoms.

The inset of Fig. 6 shows a narrow-line spectrum obtained by sweeping the clock light frequency for a 3-kHz span with bias coil current $I_{coil} = 3$ A and clock power of 2.3 mW and with 2×10^4 atoms in the lattice for 8 ms. The resulting resonance has a full-width half-maximum (FWHM) of 86(7) Hz and shows a 70% contrast.

Clock operation is enabled by locking the clock laser frequency to an absorption feature, by means of two sequential pulses separated in frequency by an amount f_{FSK}. The frequency-shifting key (FSK) modulation depth is chosen to roughly match the FWHM of the atomic resonance. The stability of the clock operation is studied by interleaving between two values of some clock parameters. Clock operations were carried on for several hours without unlocks or severe glitches. We have not observed any effect related to long-term drift of our multi-wavelength cavity which would degrade the number of atoms loaded in the lattice. A typical interleaved stability in fractional units is shown in Fig. 6. The resulting overlapping Allan deviation decreases asymptotically as $\sigma_y^{OA}(\tau) = 8.5 \times 10^{-14}\ /\sqrt{\tau}$. This means that the single-operated clock, i.e., with half averaging cycle time measurement noise, has an average asymptotic stability of $4.2 \times 10^{-14}/\sqrt{\tau}$.

The white-noise-limited clock instability can be due to the local oscillator instability via the Dick effect [31] or by shot-to-shot fluctuations of the nonnormalized number of lattice atoms. The former should be particularly limiting for our clock because of the low duty cycle (about 1.3% for a Rabi-limited resonance and 10-ms pulse). If we assume a Flicker noise floor similar to that of [36] and a white noise of 7.3 Hz^2/Hz limited by vibration noise, we get a Dick-limited Allan deviation of 4×10^{-14} at 1 s, nearly as much as the measured data.

C. Clock Frequency Shifts

Understanding the main sources of uncertainty is necessary to calibrate and test the stability of our apparatus. We have performed a preliminary evaluation of the systematic effects in our ^{88}Sr optical clock by interleaved frequency measurements. The typical measurement duration is 15 min for each point. The main sources of systematic shifts and their uncertainties are summarized in Table I.

TABLE I
PRELIMINARY ACCURACY BUDGET FOR THE TYPICAL EXPERIMENTAL CONDITIONS OF OUR ^{88}Sr CLOCK (SEE MAIN TEXT FOR DETAILS). ALL REPORTED VALUES ARE IN HZ

Effect	Shift	Uncertainty
AC Zeeman	-243.7	3.7
Probe light	-105.8	5.3
Lattice light	0	5.4
Density	1.9	0.2
BBR	-1.90	0.01
Frequency chain	0	0.02
Total:	**-349.6**	**8.4**

Because of the artificial coupling of the two clock levels in the bosonic clock, the two most important contributions to the uncertainty budget are the quadratic Zeeman shift and the light shift from the 698-nm clock laser. The associated shift coefficient are very well-known for Sr both theoretically and experimentally [18], and thus we use these values to calibrate the bias magnetic field and the probe intensity. The results are shown in Fig. 7. The quadratic Zeeman shift $\Delta\nu_B$ can be expressed as a quadratic function of the bias coils' current with an offset B_0, $\Delta\nu_B = \beta(k_{coil} I_{coil} + B_0)^2$, with $\beta = -23.8(3)$ Hz/mT^2 [37]. The measured bias coils' current calibration coefficient is $k_{coil} = 0.972(7)$ mT/A, so that for a typical value of the bias coils' current ($I_{coil} = 3$ A), the quadratic Zeeman shift induced by a bias field of 2.9 mT is resolved with an uncertainty of 3.7 Hz. The probe light shift is calibrated with a linear function resulting in a frequency shift of $-46(2)$ Hz/mW, implying a probe beam width of 158(4) μm. Thus, we can express the effective Rabi frequency as a function of the bias coil current and probe power by means of the respective induced shifts as [18]

$$\Omega_R = \xi\ I_{coil}\sqrt{P_L} \tag{2}$$

where $\xi \approx 10.6$ Hz/(A$\sqrt{\text{mW}}$).

The scalar light shift from the 813-nm lattice laser was estimated by interleaving different values of its power. The measured uncertainty at a typical working lattice depth is about 5.4 Hz due to statistical uncertainty.

Another important source of systematic uncertainty in bosonic ^{88}Sr clocks is the density shift due to collisions [38]. We performed interleaved frequency shift measurements by changing the push power of our atomic source, thus tuning the lattice loading at will, as shown in Fig. 8. Measurements span between 3.5×10^5 and 1×10^4 ^{88}Sr atoms, while both the trap depth and the atomic temperature are kept constant. Narrow-line spectroscopy with $N = 4 \times 10^4$ atoms results in a frequency uncertainty of 0.2 Hz. The resulting density shift coefficient is

$$\Delta\nu_\rho = \bar{N}_{sites}\bar{V}_{site}\frac{\delta\nu}{N} = 7(2) \times 10^{-18}\ \text{Hz}\,\text{m}^3 \tag{3}$$

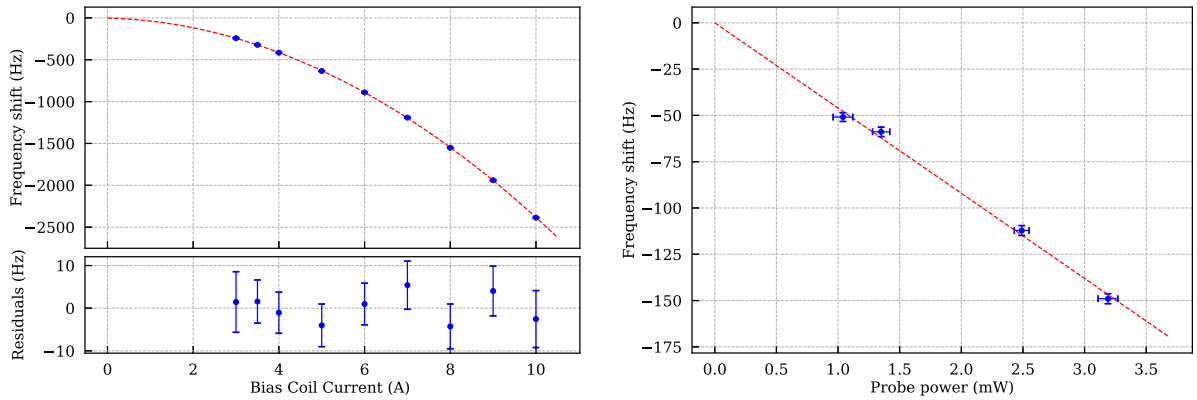

Fig. 7. Systematic study of MIS clock frequency shifts. The absolute values of both the magnetic field and the probe light intensity were calculated using coefficients from [18]. Left: Measurement of the second-order Zeeman shift as a function of the bias coil current together with fit residuals. Right: Evaluation of the probe light shift as a function of the input power.

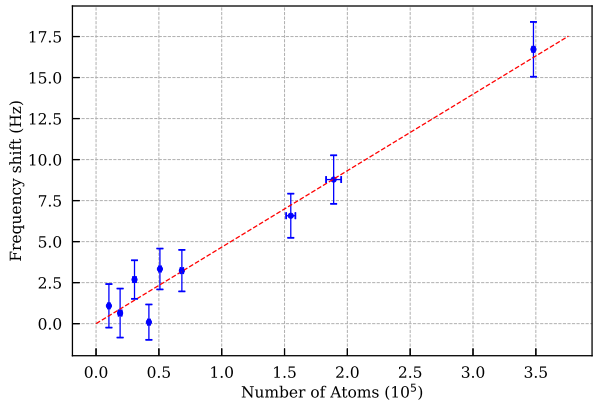

Fig. 8. Evaluation of the density shift of the ^{88}Sr clock transition. We assume linear scaling of density with atom number.

where $\bar{N}_{\text{sites}}$ is the number of occupied lattice sites, and $\bar{V}_{\text{site}}$ is the average volume occupied by the atoms in each lattice site. This depends on the lattice depth U_0 and the atomic temperatures T_r and T_z, as measured from the sideband spectroscopy (see Section IV-A) and calculated according to [39]. The uncertainty in the density coefficient is mainly due to the axial dimension estimation of the atomic sample due to the alignment of our imaging system. Compared with previous measurements [38], we found a discrepancy of a factor 3 for $\Delta\nu_\rho$.[1]

Another environmental source of frequency shift is the blackbody radiation (BBR) due to the surrounding ambient temperature T [40]. An accurate evaluation of this effect is beyond the scope of this work. We point out that the MOT/bias coils are not thermally controlled, but due to low duty cycle their effect is negligible compared with thermal fluctuations of the laboratory, which are currently controlled only within 0.5 K. The projected uncertainty in the BBR shift is 2×10^{-17} in relative units, which is completely negligible at the current level of accuracy.

[1]We recalculated the coefficient from [38] using correct expressions for $\bar{N}_{\text{sites}}$ and $\bar{V}_{\text{site}}$ according to [39]. The new value is 2.2×10^{-17} Hz m^3 assuming a temperature of 4 μK. The discrepancy can be eliminated assuming a temperature of 2 μK.

Finally, all the frequency chains driving the AOMs used for clock spectroscopy are referenced to an H-maser used for the realization of UTC(IT) timescale. The estimated uncertainty due to residual phase noise after phase-locked loop to the external reference is evaluated below 0.3 Hz at 1 s. This results in an uncertainty of 1×10^{-2} Hz for typical interleaved clock averaging times.

In summary, the total frequency accuracy is 8.4 Hz or 2×10^{-14} in relative units. It is mainly limited by the statistical uncertainty in the determination of the quadratic Zeeman shift and the probe and lattice Stark shifts.

V. Conclusion

We have described a novel apparatus for a Sr OLC based on an optically controlled cold atomic source and a multi-wavelength frequency stabilization system. These ingredients enable long periods of operation with low maintenance and high stability. Thanks to our 2D-MOT based atomic source, we have demonstrated a lifetime of 18.2(8) s in the optical lattice, remarkably longer than those obtained with Zeeman slowers.

A single reference cavity is able to properly stabilize all the lasers, resulting in an efficient and compact stabilization unit. The multi-wavelength stabilization method offers an ultimate limit on the clock laser instability at the level of $1.1(4) \times 10^{-16}/\sqrt{\tau}$ without any laser amplitude stabilization.

The resulting system is simpler and more cost-effective than previous realizations, making this design suitable for applications in challenging real-world environments [11] and for industrial grade system.

Our optical clock has shown a long-term frequency instability as low as $4 \times 10^{-14}/\sqrt{\tau}$, estimated by means of interleaved clock operation. Such limited stability is primarily affected by the short local oscillator coherence time caused by environmental vibration noise. Stable operation dominated by white frequency noise has been proven by interleaved frequency measurements for measurement times of several hours.

Technical frequency shifts have been resolved with less than 10-Hz uncertainty, limited by the short coherence time of the local oscillator and by the relatively short averaging time.

The system described in this work offers much room for improvements, both regarding short-term clock stability and long-term clock operation. The short-term stability would immediately benefit from adding a commercially available antivibration system for the reference cavity and by reducing the cycle dead-time by implementing a parallel data processing of the CCD data. These two simple changes should lower the clock instability by more than a factor 10. Long-term clock operation would require an active compensation of the multi-wavelength drift affecting the lattice loading process and the addition of automated locking algorithms for all the necessary lasers. Finally, a complete accuracy assessment of the system will require a better control of the room temperature and all clock components to correctly quantify the impact of the BBR shift.

Immediate gain in frequency stability can also be obtained by optical frequency comb-assisted spectral purity transfer [41] using the more stable optical local oscillator available for INRIM's Yb clock [42]. Fast and stable clock operations are also key ingredients to study quantum-enhanced technologies to be implemented in the newly designed science cell [43]. The upgraded system can also test active generation of a frequency standard using its sideband-enhanced cold atomic beam [44].

ACKNOWLEDGMENT

The authors would like to thank F. Bregolin and G. Barontini for careful reading of the article and M. Bober for useful discussions.

REFERENCES

[1] S. L. Campbell *et al.*, "A Fermi-degenerate three-dimensional optical lattice clock," *Science*, vol. 358, no. 6359, pp. 90–94, Oct. 2017, doi: 10.1126/science.aam5538.

[2] M. Schioppo *et al.*, "Ultrastable optical clock with two cold-atom ensembles," *Nature Photon.*, vol. 11, no. 1, pp. 48–52, 2017.

[3] K. Beloy *et al.*, "Frequency ratio measurements at 18-digit accuracy using an optical clock network," *Nature*, vol. 591, no. 7851, pp. 564–569, Mar. 2021, doi: 10.1038/s41586-021-03253-4.

[4] F. Riehle, "Towards a redefinition of the second based on optical atomic clocks," *Comptes Rendus Phys.*, vol. 16, pp. 506–515, Jun. 2015. [Online]. Available: https://www.sciencedirect.com/science/article/pii/S1631070515000638

[5] I. Ushijima, M. Takamoto, M. Das, T. Ohkubo, and H. Katori, "Cryogenic optical lattice clocks," *Nature Photon.*, vol. 9, no. 3, pp. 185–189, Mar. 2015, doi: 10.1038/nphoton.2015.5.

[6] R. Schwarz *et al.*, "Long term measurement of the ^{87}Sr clock frequency at the limit of primary Cs clocks," *Phys. Rev. Res.*, vol. 2, no. 3, Aug. 2020, Art. no. 033242, doi: 10.1103/physrevresearch.2.033242.

[7] I. S. Madjarov *et al.*, "An atomic-array optical clock with single-atom readout," *Phys. Rev. X*, vol. 9, no. 4, Dec. 2019, Art. no. 041052, doi: 10.1103/physrevx.9.041052.

[8] A. W. Young *et al.*, "Half-minute-scale atomic coherence and high relative stability in a tweezer clock," *Nature*, vol. 588, no. 7838, pp. 408–413, Dec. 2020, doi: 10.1038/s41586-020-3009-y.

[9] H. Miyake, N. C. Pisenti, P. K. Elgee, A. Sitaram, and G. K. Campbell, "Isotope-shift spectroscopy of the $^1S_0 \rightarrow {}^3P_1$ and $^1S_0 \rightarrow {}^3P_0$ transitions in strontium," *Phys. Rev. Res.*, vol. 1, no. 3, Nov. 2019, Art. no. 033113, doi: 10.1103/physrevresearch.1.033113.

[10] J. Grotti *et al.*, "Geodesy and metrology with a transportable optical clock," *Nature Phys.*, vol. 14, pp. 437–441, May 2018, doi: 10.1038/s41567-017-0042-3.

[11] M. Takamoto *et al.*, "Test of general relativity by a pair of transportable optical lattice clocks," *Nature Photon.*, vol. 14, no. 7, pp. 411–415, Apr. 2020, doi: 10.1038/s41566-020-0619-8.

[12] T. Bothwell *et al.*, "Resolving the gravitational redshift across a millimetre-scale atomic sample," *Nature*, vol. 602, no. 7897, pp. 420–424, 2022, doi: 10.1038/s41586-021-04349-7.

[13] A. Nevsky *et al.*, "Robust frequency stabilization of multiple spectroscopy lasers with large and tunable offset frequencies," *Opt. Lett.*, vol. 38, no. 22, pp. 4903–4906, Nov. 2013. [Online]. Available: http://www.osapublishing.org/ol/abstract.cfm?URI=ol-38-22-4903

[14] N. Ohmae *et al.*, "Transportable strontium optical lattice clocks operated outside laboratory at the level of 10^{-18} uncertainty," *Adv. Quantum Technol.*, vol. 4, no. 8, May 2021, Art. no. 2100015.

[15] G. Milani *et al.*, "Multiple wavelength stabilization on a single optical cavity using the offset sideband locking technique," *Opt. Lett.*, vol. 42, no. 10, p. 1970, May 2017.

[16] K. Gibble, "Scattering of cold-atom coherences by hot atoms: Frequency shifts from background-gas collisions," *Phys. Rev. Lett.*, vol. 110, no. 18, May 2013, Art. no. 180802, doi: 10.1103/PhysRevLett.110.180802.

[17] M. Barbiero, M. G. Tarallo, D. Calonico, F. Levi, G. Lamporesi, and G. Ferrari, "Sideband-enhanced cold atomic source for optical clocks," *Phys. Rev. A, Gen. Phys.*, vol. 13, no. 1, Jan. 2020, Art. no. 014013, doi: 10.1103/physrevapplied.13.014013.

[18] A. Taichenachev, V. Yudin, C. Oates, C. Hoyt, Z. Barber, and L. Hollberg, "Magnetic field-induced spectroscopy of forbidden optical transitions with application to lattice-based optical atomic clocks," *Phys. Rev. Lett.*, vol. 96, no. 8, Mar. 2006, Art. no. 083001, doi: 10.1103/PhysRevLett.96.083001.

[19] M. Takamoto, F.-L. Hong, R. Higashi, and H. Katori, "An optical lattice clock," *Nature*, vol. 435, pp. 321–324, May 2005.

[20] Corning. *See Corning Technical Brochure*. Accessed: 2006. [Online]. Available: https://www.corning.com/worldwide/en/products/advanced-optics/product-materials/semiconductor-laser-optic-components/ultra-low-expansion-glass.html

[21] J. I. Thorpe, K. Numata, and J. Livas, "Laser frequency stabilization and control through offset sideband locking to optical cavities," *Opt. Exp.*, vol. 16, no. 20, p. 15980, Sep. 2008.

[22] T. Akatsuka, M. Takamoto, and H. Katori, "Optical lattice clocks with non-interacting bosons and fermions," *Nature Phys.*, vol. 4, no. 12, pp. 954–959, Dec. 2008, doi: 10.1038/nphys1108.

[23] S. Häfner *et al.*, "8×10^{-17} fractional laser frequency instability with a long room-temperature cavity," *Opt. Lett.*, vol. 40, no. 9, p. 2112, May 2015.

[24] H. Katori, T. Ido, Y. Isoya, and M. Kuwata-Gonokami, "Magneto-optical trapping and cooling of strontium atoms down to the photon recoil temperature," *Phys. Rev. Lett.*, vol. 82, no. 6, pp. 1116–1119, Feb. 1999, doi: 10.1103/PhysRevLett.82.1116.

[25] J. L. Hall, M. S. Taubman, and J. Ye, "Laser stabilization," in *Handbook of Optics*, vol. 4. New York, NY, USA: McGraw-Hill, 2001, ch. 27.

[26] T. Nazarova, "Vibration-insensitive reference cavity for an ultra-narrow-linewidth laser," *Appl. Phys. B, Lasers Opt.*, vol. 83, pp. 531–536, May 2006.

[27] F. Acernese *et al.*, "Properties of seismic noise at the virgo site," *Classical Quantum Gravity*, vol. 21, no. 5, pp. S433–S440, Feb. 2004, doi: 10.1088/0264-9381/21/5/008.

[28] M. G. Tarallo, N. Poli, M. Schioppo, D. Sutyrin, and G. M. Tino, "A high-stability semiconductor laser system for a ^{88}Sr-based optical lattice clock," *Appl. Phys. B, Lasers Opt.*, vol. 103, no. 1, pp. 17–25, Apr. 2011.

[29] M. Barbiero *et al.*, "INRIM Sr optical clock: An optically loaded apparatus for high-stability metrology," in *Proc. Joint Conf. Eur. Freq. Time Forum IEEE Int. Freq. Control Symp. (EFTF/IFCS)*, Jul. 2021, p. 7233.

[30] J. Bergquist, W. Itano, and D. Wineland, "Laser stabilization to a single ion," in *Frontiers in Laser Spectroscopy*, T. Hansch and M. Inguscio, Eds. Haarlem, The Netherlands: North Holland, 1992, pp. 359–376.

[31] A. Quessada, R. P. Kovacich, I. N. Courtillot, A. Clairon, G. Santarelli, and P. Lemonde, "The dick effect for an optical frequency standard," *J. Opt. B, Quantum Semiclass. Opt.*, vol. 5, no. 2, pp. S150–S154, Apr. 2003.

[32] R. Grimm, M. Weidemüller, and Y. B. Ovchinnikov, "Optical dipole traps for neutral atoms," *Adv. At., Mol., Opt. Phys.*, vol. 42, pp. 95–170, Jan. 2000.

[33] S. Dörscher, R. Schwarz, A. Al-Masoudi, S. Falke, U. Sterr, and C. Lisdat, "Lattice-induced photon scattering in an optical lattice clock," *Phys. Rev. A, Gen. Phys.*, vol. 97, no. 6, Jun. 2018, Art. no. 063419, doi: 10.1103/physreva.97.063419.

[34] M. Barbiero, "Novel techniques for a strontium optical lattice clock," Ph.D. dissertation, Dept. Electron. Telecommun., Politecnico Turin, Turin, Italy, 2019. [Online]. Available: http://hdl.handle.net/11583/2750550

[35] S. Blatt *et al.*, "Rabi spectroscopy and excitation inhomogeneity in a one-dimensional optical lattice clock," *Phys. Rev. A, Gen. Phys.*, vol. 80, no. 5, Nov. 2009, Art. no. 052703, doi: 10.1103/PhysRevA.80.052703.

[36] M. Pizzocaro *et al.*, "Realization of an ultrastable 578-nm laser for an Yb lattice clock," *IEEE Trans. Ultrason., Ferroelectr., Freq. Control*, vol. 59, no. 3, pp. 426–431, Mar. 2012.

[37] T. L. Nicholson *et al.*, "Systematic evaluation of an atomic clock at 2×10^{-18} total uncertainty," *Nature Commun.*, vol. 6, no. 1, pp. 1–8, Nov. 2015.

[38] C. Lisdat, J. S. R. V. Winfred, T. Middelmann, F. Riehle, and U. Sterr, "Collisional losses, decoherence, and frequency shifts in optical lattice clocks with bosons," *Phys. Rev. Lett.*, vol. 103, no. 9, Aug. 2009, Art. no. 090801.

[39] M. D. Swallows *et al.*, "Operating a ^{87}Sr optical lattice clock with high precision and at high density," *IEEE Trans. Ultrason., Ferroelectr., Freq. Control*, vol. 59, no. 3, pp. 416–425, Mar. 2012.

[40] S. G. Porsev and A. Derevianko, "Multipolar theory of blackbody radiation shift of atomic energy levels and its implications for optical lattice clocks," *Phys. Rev. A, Gen. Phys.*, vol. 74, no. 2, Aug. 2006, Art. no. 020502.

[41] C. Hagemann *et al.*, "Providing 10^{-16} short-term stability of a 1.5μm laser to optical clocks," *IEEE Trans. Instrum. Meas.*, vol. 62, no. 6, pp. 1556–1562, Jun. 2013.

[42] P. Barbieri, C. Clivati, M. Pizzocaro, F. Levi, and D. Calonico, "Spectral purity transfer with 5×10^{-17} instability at 1 s using a multibranch Er:Fiber frequency comb," *Metrologia*, vol. 56, no. 4, Jul. 2019, Art. no. 045008, doi: 10.1088/1681-7575/ab2b0f.

[43] M. G. Tarallo, "Toward a quantum-enhanced strontium optical lattice clock at inrim," *EPJ Web Conf.*, vol. 230, Oct. 2020, Art. no. 00011, doi: 10.1051/epjconf/202023000011.

[44] H. Liu *et al.*, "Rugged mHz-linewidth superradiant laser driven by a hot atomic beam," *Phys. Rev. Lett.*, vol. 125, no. 25, Dec. 2020, Art. no. 253602, doi: 10.1103/PhysRevLett.125.253602.

Matteo Barbiero was born in Vicenza, Italy, in 1991. He received the master's degree in physics from the University of Trento, Trento, Italy, in 2015, and the Ph.D. degree in metrology from the Politecnico di Torino, Turin, Italy, in 2019.

He is currently a Post-Doctoral Research Fellow with the Istituto Nazionale di Ricerca Metrologica, Turin. His research interest includes realization of an optical lattice clock based on strontium atoms.

Davide Calonico received the Ph.D. degree in metrology from the Politecnico di Torino, Turin, Italy, in cotutoric with Pierre and Marie University, Paris, France, in 2003.

He worked on cesium fountain frequency standards in Turin and Paris. He developed ytterbium and strontium optical clocks at the Istituto Nazionale di Ricerca Metrologica (INRIM), Turin. He realized the fiber optic infrastructure in Italy, called Italian Quantum backbone, 1850-km long and covering all the countries. He is currently the Head of the Quantum Metrology and Nanotechnology Division, INRIM, including the sectors of quantum optics and time and frequency. He is also a Senior Researcher with the Time and Frequency Group. He has coordinated European and Italian funded projects and has been a PI in more than 20 funded projects. He has coauthored more than 60 articles on JCR journals (3600 citations, H-index 30 on Google Scholar).

Dr. Calonico is the Chair for the Advanced Time and Frequency Transfer (ATFT) Working Group of the International Committee for Weights and Measures (CIPM). For ten years, he has been the Italian representative at the Technical Committee for T/F at Euramet, the European Association of Metrology.

Filippo Levi received the master's degree in physics from the University of Turin, Turin, Italy, in 1992, and the Ph.D. degree in metrology from the Politecnico di Torino, Turin, in 1996.

Since 1995, he has been a Researcher with the Time and Frequency Division, Istituto Nazionale di Ricerca Metrologica (INRIM), Turin, where he is responsible for the realization of the Italian cesium fountain primary frequency standard. His other main research field is the study of cell frequency standard and in particular the study of the coherent population trapping (CPT) phenomena. In 1998 and then in 2000 and 2001, he was a Guest Researcher at the National Institute of Standards and Technology (NIST), Gaithersburg, MD, USA, for studies on the application of cooling technique to atomic frequency standards. His research interests include realization of atomic frequency standards in the microwave region and development of laser-cooled frequency standard.

Dr. Levi received the European Frequency and Time Young Scientist Award in 1999.

Marco G. Tarallo was born in Enna, Italy, in 1981. He received the Ph.D. degree in applied physics from the University of Pisa, Pisa, Italy, in 2009.

Since 2016, he has been a Researcher with the Time and Frequency Division, Istituto Nazionale di Ricerca Metrologica (INRIM), Turin, Italy. He has also worked at the LIGO Laboratories, California Institute of Technology, Pasadena, CA, USA; the European Gravitational wave Observatory, Cascina, Italy; the European Laboratory for Non-Linear Spectroscopy (LENS), Florence, Italy; and Columbia University, New York, NY, USA.